Application of Finite Element Methods to the Analysis of Stresses in Television Picture Tubes

R. E. Enstrom, R. S. Stepleman, and J. R. Appert

RCA Laboratories, Princeton, N.J. 08540

Abstract—The finite element method has been used to calculate the stress distribution and deformation behavior in a 25-inch diagonal television bulb for various design parameter changes, tension-band variations, thermal gradients during processing, and missile impact simulation. In cases where experimental results could be compared with the calculated stress distributions, the agreement was excellent. The calculations show that in a television bulb the critical stress location is on the viewing surface at the top and bottom edges of the picture (screen edge at the end of the minor axis). The tensile stress at this location is reduced by 450 psi as the amount of extra glass at the screen edge (wedge) is increased from 0 to 0.100 inch; is reduced by 75 psi as the centerface thickness is increased from 0.485 to 0.500 inch; is reduced by 40 psi and increased by 90 psi for a bulge or a notch, respectively, at the interior screen edge; is increased by 10 psi for a spun ($\frac{1}{3}$ thinner) rather than a pressed funnel; is unchanged for a broader funnel than panel seal edge; is reduced by up to 235 psi by offsetting the panel from the funnel seal edge (but this increases the frit seal stress by a factor of 4 to 5 times); is reduced by 150 psi for a tension band positioned near the face; is reduced by about 300 psi for two overlayed tension bands; is increased to about 12,000 psi during UL missile impact testing of an unbanded (nonprotected) bulb; and is reduced to 1200 psi *compressive* stress during heat up in the vacuum bake cycle.

1. Introduction

The finite element method is a powerful tool in the analysis of structures for static stress distributions, dynamic response, heat transfer, and fluid flow, and for interactions between these four parameters. In brief, finite element analysis is a means of subdividing a complex solid continuum into discrete blocks (finite elements) for which mathematical formulas

can be derived that describe their behavior. The aggregate structure is the sum of the properties of these individual blocks (elements) and their interactions. Each solid block can have 8 corners (or nodes) and each node can move in any of three directions (x, y, and z). Accordingly, for an assemblage of 300 elements used to describe a television picture tube, there might be on the order of 1600 simultaneous equations used to describe the response of the tube to atmospheric pressure upon evacuation of the interior of the tube. The solution of this large number of equations requires matrix methods and the use of large scale digital computers.

The power of the method is that it permits the *a priori* estimate of a stress distribution, frequency of vibration, etc., from a descriptive blueprint of the geometry of the structure and the elastic properties of the materials constituting the structure. In this way, many design changes can be made, and the effect of these design changes on the stress distribution can be evaluated before any metal is cut for a mold or a large scale structure assembled.

The basic equations used in the finite element method are given below. Here the forces and displacements are calculated for the element corners, called nodes. A force acting on a node causes a displacement. The set of force–displacement equations for one finite element having n-degrees of freedom is[5]

$$\begin{aligned} F_1 &= k_{11}\Delta_1 + k_{12}\Delta_2 + \ldots + k_{1j}\Delta_j + k_{1n}\Delta_n \\ &\vdots \\ F_i &= k_{i1}\Delta_1 + k_{i2}\Delta_2 + \ldots + k_{ij}\Delta_j = k_{in}\Delta_n \\ &\vdots \\ F_n &= k_{n1}\Delta_1 + k_{n2}\Delta_2 + \ldots + k_{nj}\Delta_j + k_{nn}\Delta_n. \end{aligned} \qquad [1]$$

Here k_{ij} is an element stiffness coefficient and Δ_j is the displacement at the jth node. These nodal forces and displacements are summarized in the element stiffness equation

$$\{F\} = [k]\{\Delta\}, \qquad [2]$$

which represents the array of linear algebraic equations given in Eq. [1]. Here, $[k]$ is the element stiffness matrix (consisting of the material-dependent elastic stiffness matrix, the degree-of-freedom-to-strain transformation, and the stress-to-force transformation). $\{F\}$ and $\{\Delta\}$ are the element force and displacement vectors, respectively. The nodal displacements are the unknowns.

The matrices for the individual elements are next combined to form a complete set of equations for all the elements in the full structure (global) taking into account equilibrium, boundary, and continuity of nodal displacement conditions. This is given as the global stiffness equation,

$$\{P\} = [K]\{\Delta\}, \qquad [3]$$

where $[K]$ is the global stiffness coefficient matrix for all the elements, $\{P\}$ is the vector of global nodal forces (due to the summation of applied loads, atmospheric pressure, etc.) and $\{\Delta\}$ is the vector of nodal point displacements, as before. The general solution to Eq. [3] is obtained by a sophisticated technique for solving systems of linear equations. However, we can think of this symbollically as obtaining the displacement by

$$\{\Delta\} = [K]^{-1}\{P\}. \tag{4}$$

The element stresses are obtained from the displacement by[5]

$$\{\sigma^i\} = [S^i]\{\Delta^i\}, \tag{5}$$

where $\{\sigma^i\}$ is a vector giving the stress at specified points in the ith element, $[S^i]$ is the element stress matrix, and $\{\Delta^i\}$ represents the displacements for the ith element. Δ can consist of as many as three components, u_x, u_y, and u_z expressed as a polynomial expansion in terms of the Cartesian coordinates, x, y, and z.

$$\begin{aligned} u_x &= a_1 + a_2 x \\ u_y &= a_3 + a_4 y \\ u_z &= a_5 + a_6 z. \end{aligned} \tag{6}$$

For the particular isoparametric finite element used in the present calculations (see Sec. 2), the polynomials are[6]

$$\begin{aligned} u_x &= \sum_{i=1}^{8} h_i u_{xi} + h_9\alpha_{x1} + h_{10}\alpha_{x2} + h_{11}\alpha_{x3} \\ u_y &= \sum_{i=1}^{8} h_i u_{yi} + h_9\alpha_{y1} + h_{10}\alpha_{y2} + h_{11}\alpha_{y3} \\ u_z &= \sum_{i=1}^{8} h_i u_{zi} + h_9\alpha_{z1} + h_{10}\alpha_{z2} + h_{11}\alpha_{z3}. \end{aligned} \tag{7}$$

Here α_i is the displacement amplitude and is an additional degree of freedom. The coefficients represent the interpolation functions and are given by

$$\begin{aligned} h_1 &= \frac{1}{8}(1+\xi)(1+\eta)(1+\zeta), \quad h_2 = \frac{1}{8}(1-\xi)(1+\eta)(1+\zeta) \\ h_3 &= \frac{1}{8}(1-\xi)(1-\eta)(1+\zeta), \quad h_4 = \frac{1}{8}(1+\xi)(1-\eta)(1+\zeta) \\ h_5 &= \frac{1}{8}(1+\xi)(1+\eta)(1-\zeta), \quad h_6 = \frac{1}{8}(1-\xi)(1+\eta)(1-\zeta) \\ h_7 &= \frac{1}{8}(1-\xi)(1-\eta)(1-\zeta), \quad h_8 = \frac{1}{8}(1+\xi)(1-\eta)(1-\zeta) \end{aligned} \tag{8}$$

$$h_9 = (1 - \xi^2), \quad h_{10} = (1 - \eta^2),$$
$$h_{11} = (1 - \zeta^2).$$

Here ξ, η, and ζ are nondimensional local coordinates in the range -1 to $+1$. The first eight coefficients are the usual compatible interpolation functions. Coefficients 9, 10, and 11 are the *incompatible* interpolation functions that are related to linear shear and normal strains.[6] These incompatible displacement modes are introduced in improved elements (i.e., isoparametric) to enhance the accuracy by permitting the element edges to bend, as compared to lower-order, constant-strain, compatible elements that cannot bend along the element edges, but can only translate.

Compared with constant-strain elements, the isoparametric element shows a significant improvement in the accuracy of the finite element solution. For example, while a constant-strain element might result in a solution for displacement or bending stress of a cantilever within 30% of the exact solution values, the isoparametric element having incompatible modes results in values virtually identical with the exact solution.[6] Further, in three dimensions, elements having incompatible displacement modes, which improve the element bending characteristics and solution accuracy, have been found to be excellent for the analysis of large structures such as dams and thick pipes.[6] In fact, accurate solutions can be achieved using only a single element to describe the thickness, which significantly reduces the computer time required compared to that using multi-elements through the thickness. A single element is used for the thickness in the present kinescope finite element model.

2. Experimental Procedure

The ANSYS[7] finite element computer program (Revision 2) in conjunction with a Control Data Corporation 7600 computer was used for all of the calculations reported here. The finite element model of the 25 V 90° tube was developed from the blueprints of the standard panel and funnel shown in Figs. 1 and 2. A total of 267 isoparametric three-dimensional elements (ANSYS STIF 45) were used to describe the tube structure. This element has eight nodal points, each having translational degrees of freedom in the x, y, and z directions. As shown in Fig. 1, the vacuum side of the viewing area is spherical and the outside is nonspherical. This geometry results in differing glass thickness in the three principal directions along the tube surface, i.e., the major, minor, and diagonal axes. The funnel has been modeled to represent a pressed glass funnel having an approximate wall thickness of 0.25 inches or a spun-glass funnel having a wall thickness of about 0.170 inches. The frit seal

between the panel and the funnel was modeled as an element 0.010 inches thick by 0.35 inches wide by about 1 inch long.

The Cartesian coordinates for the element nodes were calculated from the radii of curvature specified for a 25 V 90° picture tube (Fig. 1) and these are: inside vacuum surface R = 40.7 inches; outside minor axis R = 44.794 inches; outside major axis R = 42.123 inches; and outside diagonal axis R = 41.704 inches. The panel skirt and funnel node points were determined graphically from full-size blue prints.

The materials properties are given in Table 1. With the input data for the materials properties, the element description, and the Cartesian coordinates for the nodal points, the ANSYS software program was used to generate the element surface stresses, element deflections, and graphical representations of the picture-tube deformation resulting from the action of atmospheric pressure on an evacuated tube. The surface

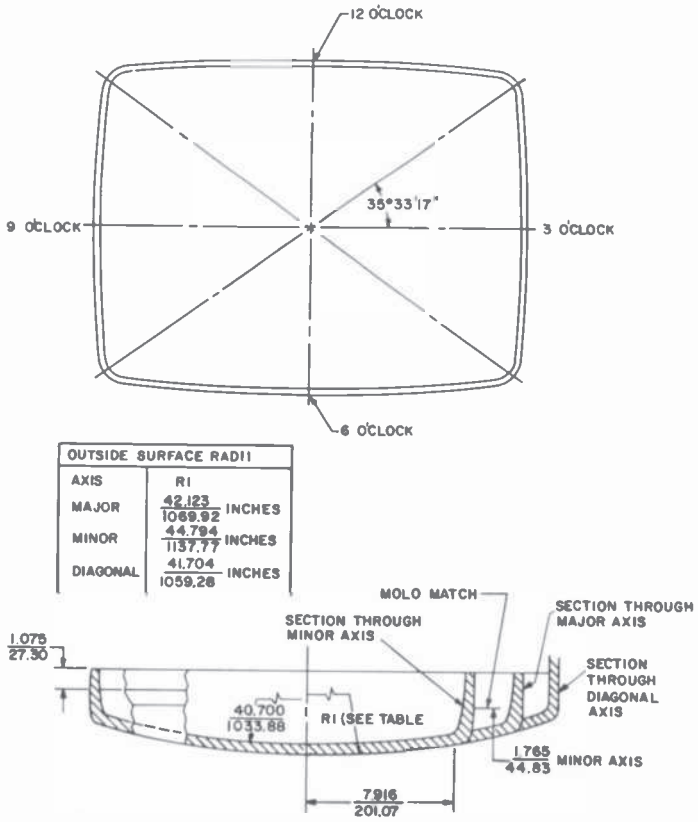

Fig. 1—Top and side views of a standard 25 V 90° panel. Width of seal edge is 0.350 inches. Radii of curvature for inside and outside surfaces are shown.

Table 1—Materials Properties

	Young's Modulus (psi)	Poisson's Ratio	Expansion Coefficient ($°C^{-1}$)	Density ($lb.\ Mass/in^3$)
panel & funnel glass	10×10^6	0.223	98.5×10^{-7}	3.03×10^{-3}
frit seal	7×10^6	0.29	97.5×10^{-7}	7.24×10^{-3}

stress printout contains information on the two principal stresses and their directions. In the figures describing the stresses in the various parts of the picture tube, the algebraically largest value of the two principal stresses is reported. *Thus, these figures show the largest compressive or tensile stresses for each element.*

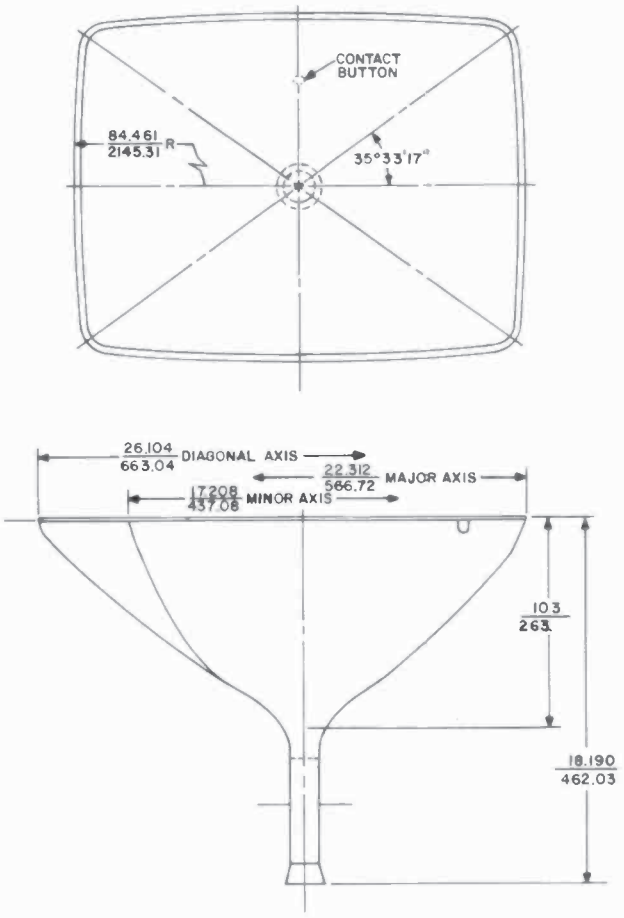

Fig. 2—Top and side views of standard 25 V 90° funnel.

3. Results and Discussion

The stress distribution was calculated for a standard 25 V 90° tube subjected to atmospheric pressure loading. In addition, the effect of other variables on the stress distribution was calculated. These variables included the effect of:

1. varying amounts of glass thickness near the edge of the tube (wedge),
2. altering the center face thickness,
3. altering the blend radius,
4. reducing the funnel thickness,
5. using a broader funnel than panel seal edge,
6. offsetting the panel and funnel seal edges,
7. altering the tension band location,
8. incorporating double tension bands,
9. simulating the Underwriters' Laboratories missile impact test,
10. incorporating thermal gradients (e.g., during tube processing).

These areas are described in detail in the following sections. First, however, the stress distribution calculated for a standard tube is presented.

3.1 Standard 25 V 90° Tube Model

The finite element model for a quarter section of the 25 V 90° panel is shown in Fig. 3. Only a quarter section is needed to describe the panel, since the panel is symmetrical about the major (horizontal) and the minor (vertical) axes as the viewer observes the panel in an operating set. The complete panel can be mathematically simulated by the inclu-

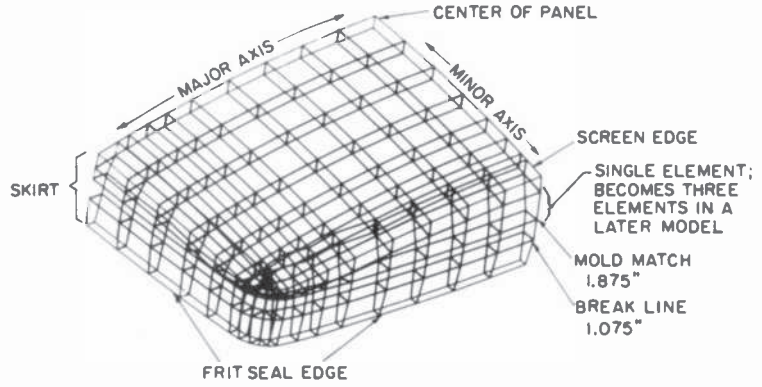

Fig. 3—Finite element model of a one quarter section of a 25 V 90° panel (Run 59B), as viewed from the inside of the tube, showing the element geometry and size.

sion of boundary conditions along the minor and major axes respectively, as $UY = 0$ and $UX = 0$ (which specify no motion in the horizontal and vertical directions). The finite element grid shown in Figs. 3 and 4 is composed of elements of differing sizes. The reason for this is to have a large number of elements in high-stress-gradient locations, and a smaller number in regions where the stress changes only gradually. Such a procedure provides accurate stress calculations at all locations while minimizing the number of elements and, therefore, the computer time/cost of the analysis.

Larger size elements are utilized towards the center of the panel, as shown in Fig. 4. The element size gradually decreases along both the minor and the major axes. At the screen edge, where the viewing surface and the skirt of the panel meet, the element size is about 0.25 inches wide, so that the stress can be accurately calculated in this high-stress-gradient region. The stress gradient along the minor axis will be illustrated in a subsequent figure. Fig. 3 also shows that the panel is a single element thick. It is only by the use of high order *isoparametric* elements (STIF 45 in ANSYS) that accurate stress distributions can be achieved using a single element. Wilson, et al.,[6] have compared plate structures and have shown that results very close to exact solutions can be calculated using a relatively small number of isoparametric elements having incompatible modes. Doubling the number of simpler, constant-strain, elements does not result in comparable accuracy.

It may also be noted in Figs. 3 and 4 that the element shape is close

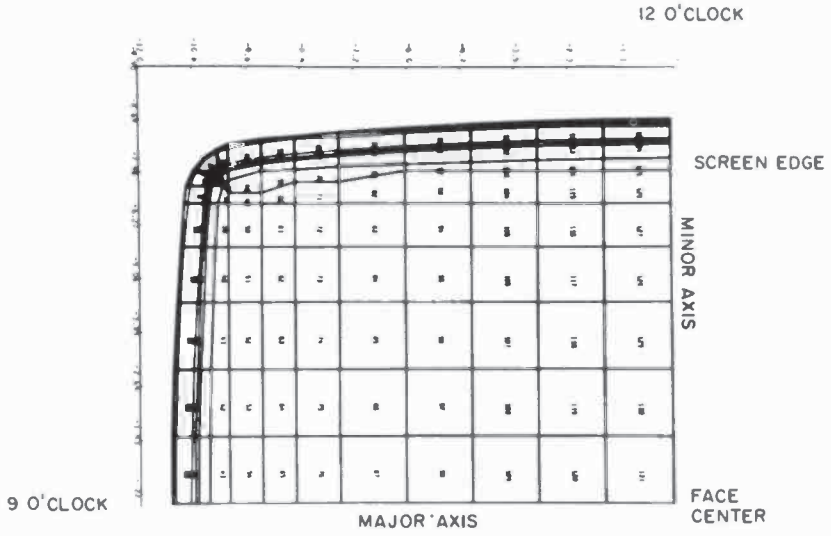

Fig. 4—Top view of a finite element model of a one-quarter section of a 25 V 90° panel.

to rectangular even in the skirt-panel intersection region; this geometry will be shown more clearly in subsequent figures showing sections through the minor axis. To achieve the highest accuracy with these 8-noded solid elements, a well-proportioned aspect ratio should be used. The recently published work of Elst and Wielanger[8] for a 26 V 110° color picture tube showed a similar type of element geometry, which they created independently from our work. Here too, rectangular solids were used in all locations, rather than wedge-shaped sections which might have been used near the screen edge and into the skirt.

Side and end views of the finite element model of the panel and funnel quarter section are shown in Figs. 5 and 6, respectively. The element numbers are shown at the center of each element. The multiplicity of lines outlining the funnel and panel outer periphery results from viewing a curved surface from the side.

In the initial model, the skirt of the panel incorporated three elements, as shown in Fig. 3. However, the one element that described the region between the mold match and the viewing surface, also indicated in Fig. 3, became quite large near the end of the minor axis. Therefore to refine the model of the skirt in this region, the one large element was subdivided into three elements. These three elements, having a notation A, B, C, have principal stresses of 772, 796, and 859 psi tension, respectively, as shown in Fig. 7(a). The arithmetic average for these maximum stresses

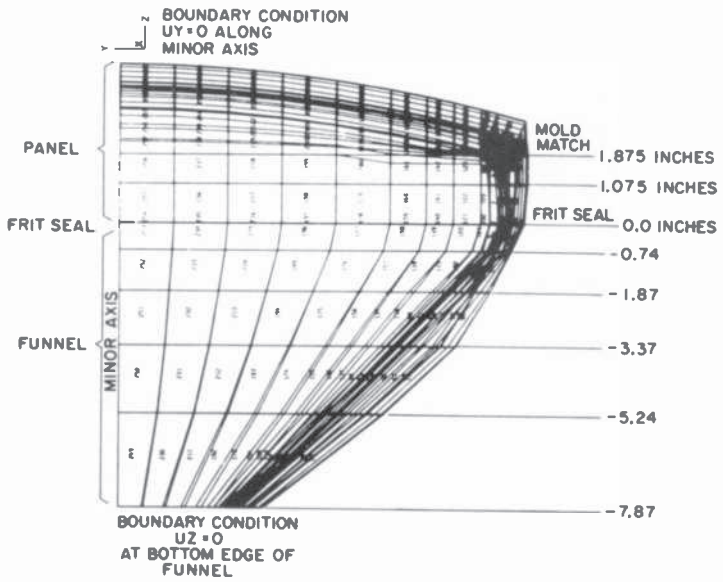

Fig. 5—Side view of a finite element model of a one-quarter section of a 25 V 90° panel and funnel (Run 63C) as viewed parallel to the minor axis.

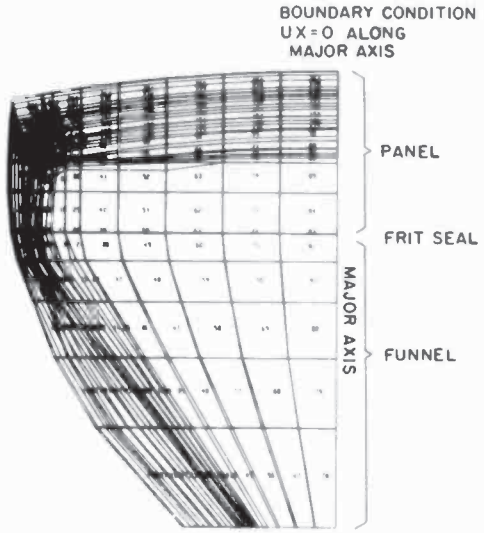

Fig. 6—End view of finite element model of a one-quarter section of a 25 V 90° panel and funnel as viewed parallel to the major axis (Run 63C).

is 809 psi, which compares well with the principal stress of 825 determined for the larger element. This shows that the subdivision better defined the gradient rather than altering it. Everywhere else the stresses are virtually the same in both models.

Next, the lower inner nodes of elements A and B were moved outward by 0.075 and by 0.038 inches, respectively, to reduce the thickness. As shown in Fig. 7(b), the stress is reduced by 25 psi to 1275 psi tension at the screen edge. In elements A, B, and C, the stress is increased somewhat compared to Fig. 7(a). Elsewhere the stresses are virtually unchanged when the skirt model is made thinner (e.g., comparing Figs. 7(a) and (b)).

Fig. 8 shows a comparison between the finite element model cross-section along the minor axis and an actual glass cross-section. Here a good correspondence is seen between the finite element model and the glass structure. Accordingly, we believe that the stresses shown in Fig. 7(b) represent a good approximation to the stress distribution in an actual panel. Because the inside of the panel model does not have a fillet, the calculated stress at the screen edge may be 100 psi higher than for an actual panel having a fillet present.

In Fig. 9, the calculated stress versus distance along the major and minor axes is shown for the atmospheric surface for Run 63C (center face thickness is 0.500 inches). Also plotted are the actual strain-gage-measured stress values,[9] and these are seen to be in excellent agreement with

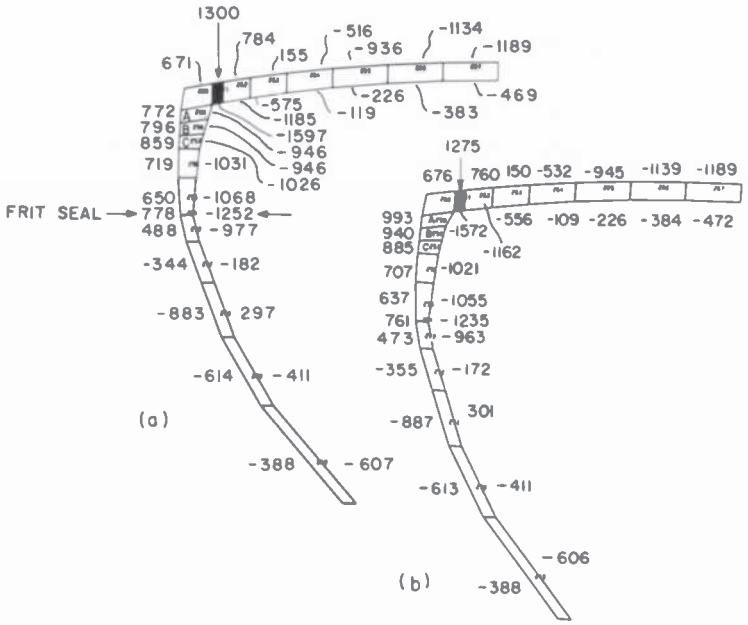

Fig. 7—(a) Cross-section through minor axis of color-tube model having straight inside edges for elements A, B, and C. Negative stresses are compressive and positive stresses are tensile. (b) Cross section through minor axis of color-tube model having a thinner skirt at elements A, B, and C (Deck 63C). Negative stresses are compressive and positive stresses are tensile.

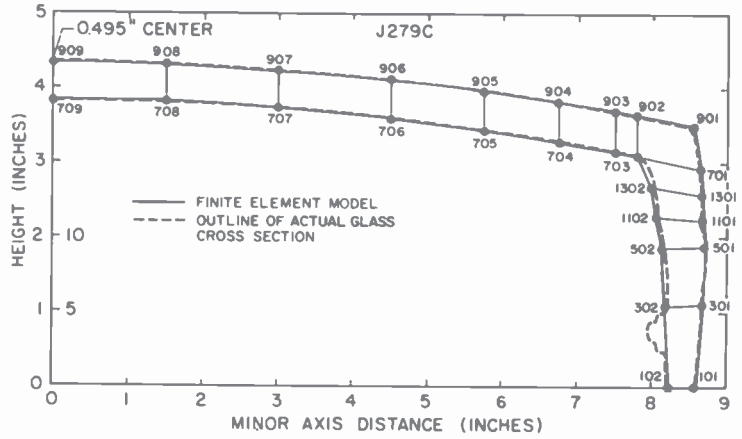

Fig. 8—Comparison of finite element model cross section (Deck 63C) through minor axis with cross section of actual 25 V 90° glass. The finite element nodes are shown and numbered.

the calculated curve. The rapid increase in stress near the screen edge requires that the strain gages be very accurately and reproducibly positioned. A difference in placement of $\frac{1}{8}$ to $\frac{1}{4}$ inch can significantly increase or decrease the observed stress (near the screen edge, $\frac{1}{4}$ inch corresponds to a stress difference of 200 psi).

Both curves in Fig. 9 show the transition from compressive stresses in the center of the panel to tensile stresses toward the edge of the panel. Along the minor axis this occurs at about 6 inches from the face center, while along the major axis the transition occurs about 9 inches from the center of the tube face. A similar type transition occurs for a beam fixed at both ends having an atmospheric pressure load.[10] In both cases, compressive forces are noted near the center portion while tensile stress is present on the top surface near the support point (a wall in the case of the beam and the skirt in the case of the television panel). The more complex panel structure has a stronger dependence of stress on distance than does a simple beam. Comparison of the stress distribution in the two limiting text-book cases of simply supported plates[11] with plates having built-in ends[12] shows that a television panel on a funnel is an in-between condition and, therefore, difficult to calculate using standard text-book type equations. Accordingly, the finite element approach to the calculation of the stress distribution is preferred, because it is not limited to specific boundary conditions. Rather the boundary conditions

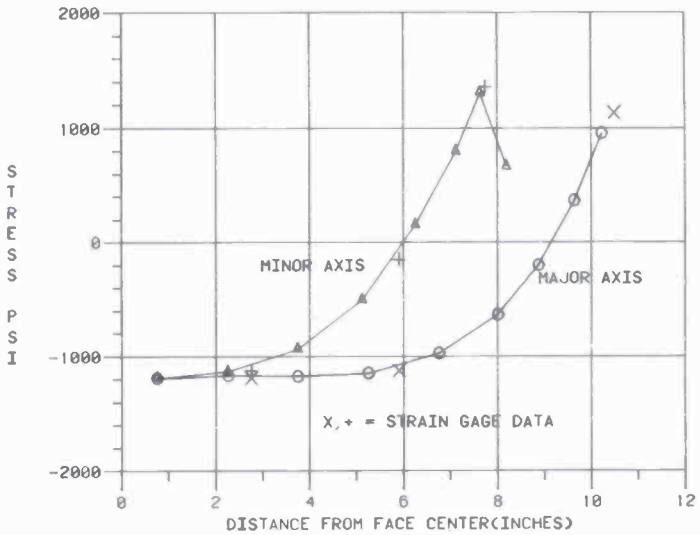

Fig. 9—Comparison of calculated stress with experimentally determined stress along the major and minor axes.

imposed by the geometry and materials properties, as in the real structure, are the ones that are operative.

The ANSYS calculated stresses and experimentally determined values are compared in Fig. 10. Here it may be seen that tensile stresses are present in the panel skirt, the frit seal, and the adjacent region of the funnel. The lower portion of the funnel exhibits only compressive stresses. The frit seal is important because it joins the panel and the funnel parts together to form the complete bulb. It is important that stresses be kept low in this region, since the frit material after firing is not as strong as the parent glass. In later sections the effect of offset between the panel and funnel mating surfaces on the frit seal stresses will be discussed.

The stresses present over the viewing area (in quarter symmetry), resulting from the atmospheric pressure acting on the evacuated bulb, are shown in Fig. 11 for the outside surface and in Fig. 12 for the vacuum side. The stresses shown for the minor axis cross-section in Fig. 7(b) are the same as along the minor axis in Figs. 11 and 12. The high-stress region along the screen edge extends from the minor axis to the corner to the major axis. This high-stress region in a tube is a very critical location and may be a cause of failure of the tube. Accordingly, it is particularly important that this region not be subject to extraordinarily high stresses resulting from the glass fabrication or mounting the tube in the cabinet. While glass is strong in compression, it is very weak in tension. Further

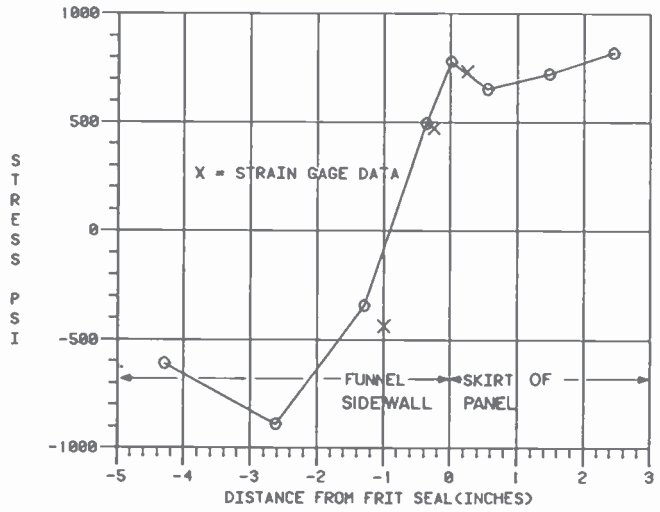

Fig. 10—Comparison of calculated stresses with experimentally determined stresses in the skirt and funnel along the minor axis.

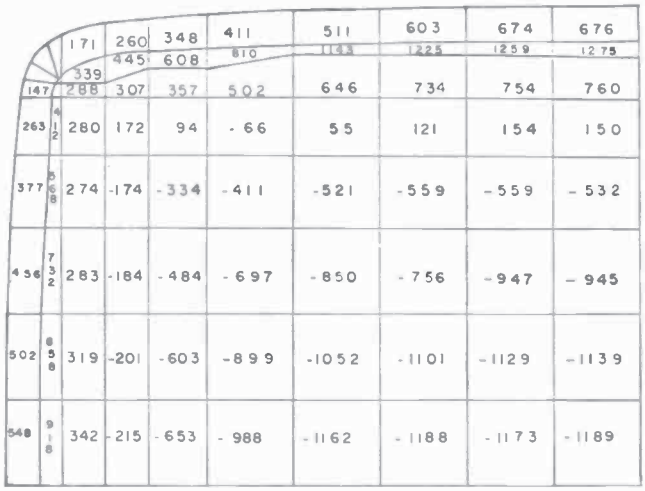

Fig. 11—Stresses present on the atmospheric side of the viewing surface resulting from atmospheric pressure (63C). Note the high stress region along the screen edge. Negative stress are compressive and positive stresses are tensile.

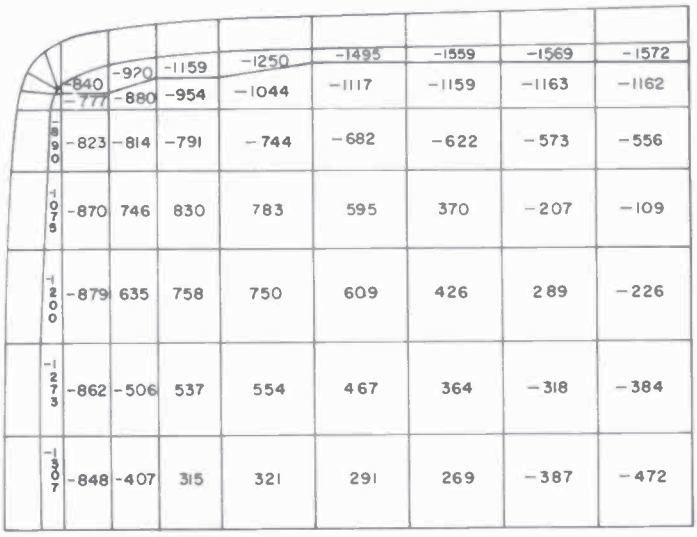

Fig. 12—Stresses present on the vacuum side of the viewing surface resulting from atmospheric pressure (Deck 63C). Negative stresses are compressive and positive stresses are tensile.

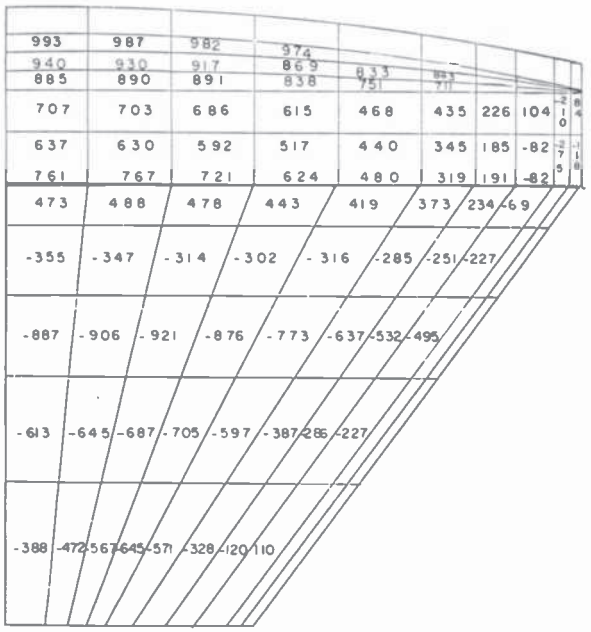

Fig. 13—Stresses present on the atmospheric side of the skirt and funnel as viewed parallel to the minor axis (63C).

it is subject to failure by a stress corrosion mechanism whereby water vapor in the air reacts with the glass at high tensile stress locations to cause premature failure. This failure mechanism is time dependent, so that the actual failure can occur some time after a surface defect has been initiated. Later sections discuss in more detail the effect of geometric changes in the glass thickness near the screen edge on the tensile stress in this location. The stresses at the screen edge on the vacuum side are all compressive and thus of no concern even though the magnitude of the stress can range up to nearly 1600 psi, as seen in Fig. 12.

The stress distribution on the skirt and funnel is shown for the atmospheric surface in Figs. 13 and 14 when viewed parallel to the minor and major axes, respectively. In Fig. 13, the tensile stresses in the skirt are seen to decrease as one proceeds in the direction of the tube corner from the end of the minor axis. Similarly, in Fig. 14, these tensile stresses are highest at the major axis and decrease towards the tube corner. In the funnel, the stresses are mainly compressive and therefore of not too much consequence, except near the frit seal. It should be pointed out that Figs. 13 and 14 refer to a pressed funnel. In a later section, results will be presented for the stress distribution in a thinner, spun-type funnel.

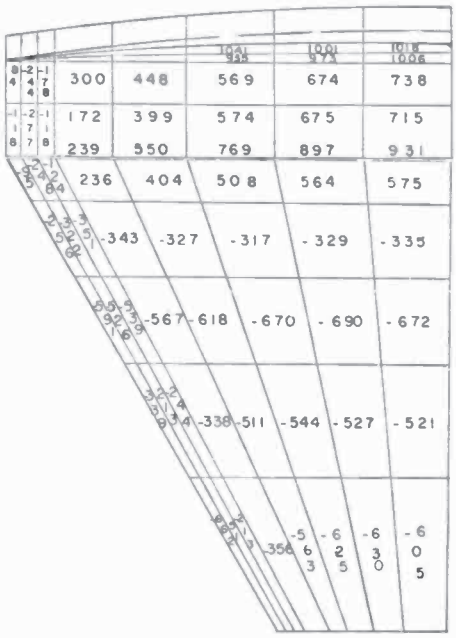

Fig. 14—Stresses present on the atmospheric side of the skirt and funnel as viewed parallel to the major axis (63C).

The stresses on the vacuum surface for the tube are shown in Figs. 15 and 16. Here, the stresses are virtually all compressive on both the skirt and funnel surfaces. These figures illustrate another advantage of the finite element analysis, i.e., that stresses can be calculated for regions, such as the inside of the tube, that are difficult to measure with strain gages.

In addition to stress distributions, the displacement of the structure under the action of the atmospheric pressure load can be calculated. In Fig. 17 the displacement calculated for atmospheric pressure acting on an evacuated bulb is illustrated. Here the center of the tube is calculated to move inward by 0.007 inches. The inward movement of the face in turn counteracts the atmospheric pressure acting on the skirt, with the result that a net outward movement of the skirt is observed. Below the frit-seal region, the action of the atmospheric pressure causes a new inward movement of the funnel, leading to a general compressive state of stress in this region. It should be pointed out here that the deformation and stresses shown in the previous series of figures represent the response of the tube only to atmospheric pressure. The effects of implosion protection bands on the response of the tubes will be illustrated later.

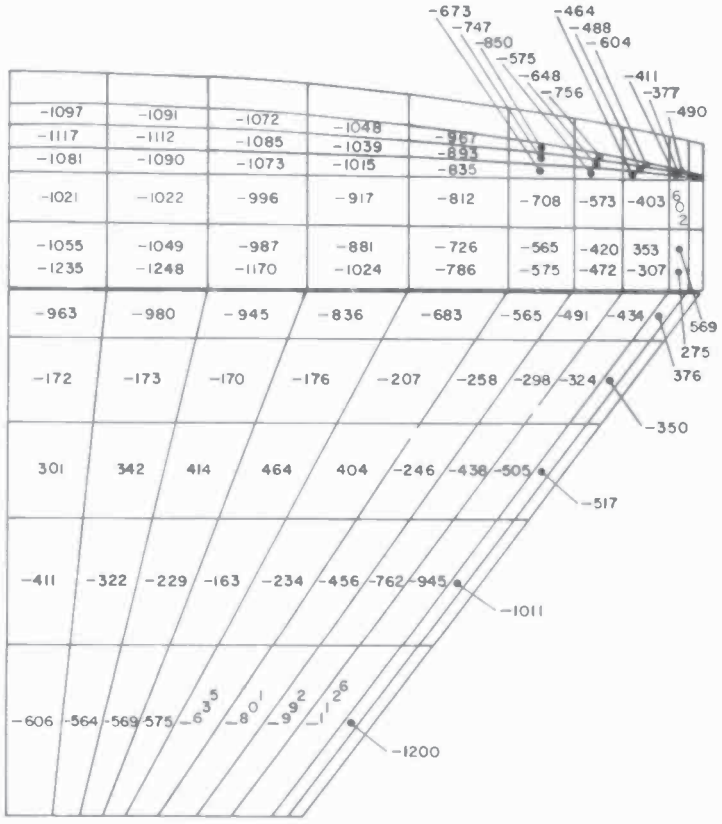

Fig. 15—Stresses present on the vacuum side of the skirt and funnel as viewed parallel to the minor axis (63C).

3.2 Effect of Wedge on Stresses

In the previous section, the wedge at the screen edge was determined by the difference of the inside and outside radii of curvature of the tube face. To try to help understand the effect of wedge (the difference in thickness at the screen edge compared to the thickness at the center of the tube face) at the minor and major axis screen edges, a standard 25 V 90° finite element model was modified to have 0, 0.050 and 0.100 inches of additional glass thickness at the screen edge. This was accomplished by keeping the inside of the viewing surface fixed at a radius of 40.7 inches while using three different *spherical* radii of curvature for the outer surface, as given in Table 2.

Since the outside surface was treated as spherically symmetric, there will be greater wedge at the ends of the major and diagonal axes than is

Table 2—Dimensions for 25V 90° Panels Having Various Amounts of Wedge

Computer Run	Inside Radius of Curvature (inches)	Outside Radius of Curvature (inches)	Wedge at Minor Axis Screen Edge* (inches)
61B	40.7	40.7	0.0
61D	40.7	43.792	0.050
61E	40.7	47.37	0.100
59C	40.7	44.794 Minor 42.123 Major 41.704 Diagonal	0.065 0.044

* 7.57 inches from face center

shown for the minor axis. For comparison, the radii of curvature for the present 25 V 90° panel are given in Table 2; here the outside surface is not spherical, which produces less wedge at the end of the major axis where the stress is lower than at the end of the minor axis. In a second type of industry-standard panel, the inside surface is pressed to a non-spherical shape and the outside viewing surface is polished to a spherical curvature. The thickness at the center of the viewing surface for the

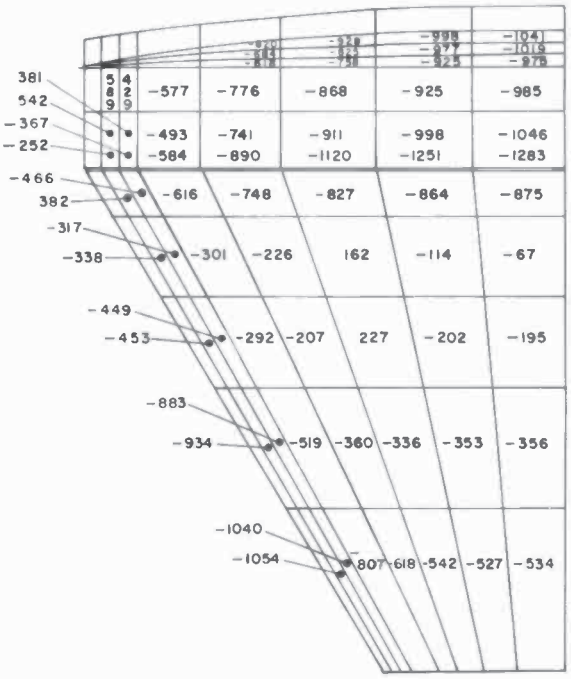

Fig. 16—Stresses present on the vacuum side of the skirt and funnel as viewed parallel to the major axis (63C).

Table 3—Results of ANSYS Computer Calculations for Stress at the Minor Axis Screen Edge

Computer Run	Wedge (inches)	Thickness at Screen Edge (inches)	Stress (psi)	Reduction of Stress (psi)	Stress in Frit Seal (psi)
61B	0.0	0.485	1610	0	734
61D	0.050	0.539	1360	250	770
61E	0.100	0.593	1168	442	793
59C	0.065	0.555	1379		775

above models was taken as 0.485 inches; for the previously shown results on Run 63C the panel thickness is 0.500 inches at face center.

The results of the ANSYS calculations are given in Table 3 for the critical area at the minor axis screen edge. More detailed data are presented in Fig. 18(a)–(c), which shows the stresses existing on both the vacuum side and atmospheric surface along the minor axis for tubes having 0.0, 0.050, and 0.100 inches of wedge, respectively. Comparison of the data in the figure suggests that differing amounts of wedge affect principally the tensile stresses at the screen edge. At this location, the stress decreases from 1610 to 1360 and then to 1168 psi as the wedge is increased from 0.0 to 0.050 and then to 0.100 inches, respectively. The dependence of the decrease in stress with increasing wedge is shown in Fig. 19. Here, the tensile stress at the screen edge is seen to decrease nearly linearly with increasing wedge. Accordingly, if strain gage mea-

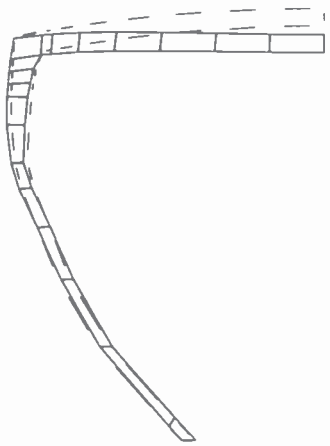

Fig. 17—Section of the color tube model through the minor axis showing the displacement calculated for atmospheric pressure acting on an evacuated bulb. The dotted line indicates the original undeformed structure. The maximum deformation at the center is 0.007 inches.

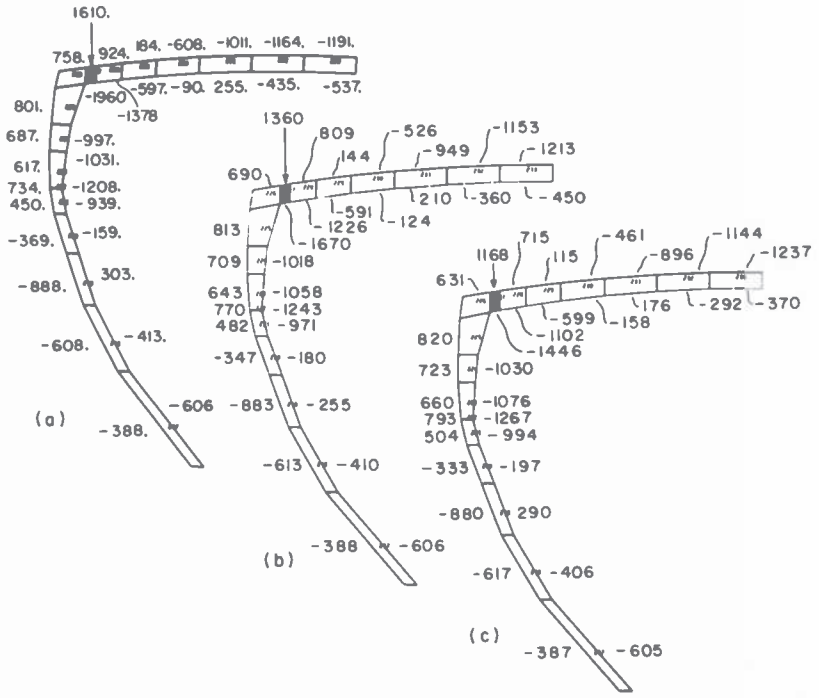

Fig. 18—Cross-section of a 25 V 90° tube (a) having a 0.485 inch center face thickness and no wedge at the minor axis screen edge (61B), (b) having a 0.485 inch center face thickness and 0.050 inches of wedge at the minor axis screen edge (61D), and (c) having a 0.485 inch center face thickness and 0.100 inches of wedge at the minor axis screen edge (61E).

surements showed higher than desired stress at the screen edge on a particular batch of tubes, the stress could be reduced significantly by building in additional wedge during the glass forming operation, or by removing less glass during the face polishing operation.

Finally, it should be noted that decreasing the stress at the screen edge by increasing the wedge makes the panel surface stiffer. This greater stiffness then tends to increase the stress in the skirt and in the frit seal. However, the increase in stress in the frit-seal region from 734 to 793 psi as the wedge increases from 0.0 to 0.1 inches is fortunately much less than the reduction in stress at the screen edge (440 psi).

3.3 Effect of Center Face Thickness on Stress

The results described above were calculations for panels having a center face thickness of 0.485 inches. This value represents the design standard thickness. Indeed, a preferable panel thickness may be 0.500

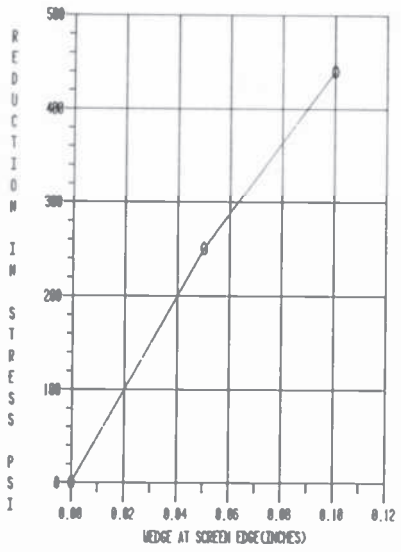

Fig. 19—Reduction in tensile stress at the minor axis screen edge as a function of wedge for a 25 V 90° panel on a pressed funnel. Both the atmospheric and vacuum viewing surfaces of the panel are spherically symmetric.

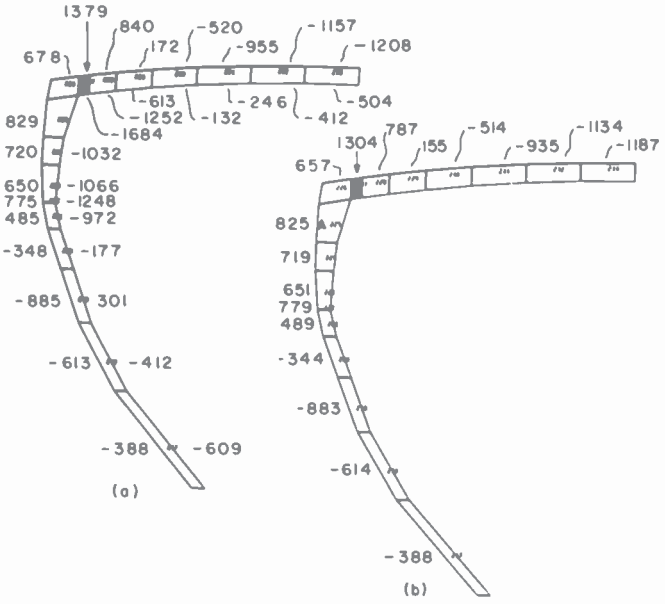

Fig. 20—Minor axis cross-section showing stresses present in tubes having (a) 0.485 inch and (b) 0.500 inch center face thicknesses (59HH).

Table 4—Comparison of Stresses at the Minor Axis Screen Edge for 0.485 and 0.500 Inch Centerface Panels

Computer Run	Centerface Thickness (inches)	Stress (psi)	Increased Thickness (inches)	Reduction in Stress (psi)
59C	0.485	1379	0	0
59HH	0.500	1304	0.015	75

inches. To make the comparison for the effect of center face thickness, the same finite element model was used and only the coordinates for the outer surface were changed. The same internal and external radii of curvature were used. The calculated stresses for the 0.485- and 0.500-inch thick panels are shown in Fig. 20. Here, the stress at the minor axis screen edge is reduced to 1304 psi (0.500 inches) from the value of 1379 psi observed for the 0.485 inch panel. Stresses at other locations on the face are also reduced, but by an increasingly smaller amount proceeding toward the center. The stresses in the funnel and skirt are virtually unchanged as the panel thickness increases (by .015 inches uniformly), in contrast to the greater skirt stresses observed in Figs. 18(a)–(c) when the wedge was increased. These results are summarized in Table 4.

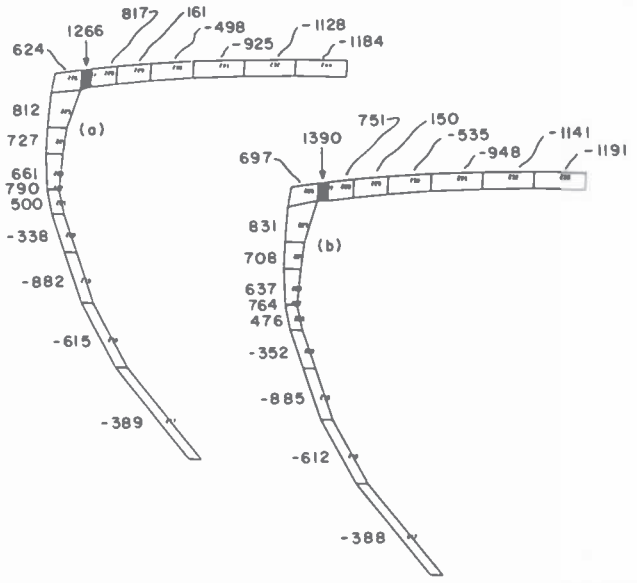

Fig. 21—Minor axis cross-sections showing stresses present in 0.500 inch center face thickness tubes having (a) a bulge or (b) a notch at the screen edge.

Table 5—Comparison of Stresses at the Minor Axis Screen Edge for Panels Having Local Increased or Decreased Thickness at this Location. Both Panels have a 0.500 Inch Centerface Thickness

Computer Run	Screen Edge Thickness (inches)	Stress (psi)	Change in Thickness (inches)	Change in Stress (psi)
62CH	0.520	1390	−0.050	+86
59HH	0.570	1304	0	0
62DH	0.620	1266	+0.050	−38

3.4 Effect of Blend Radius Geometry on Stress

The thickness of glass at the screen edge was varied to determine the effect on the stress of a localized notch or bulge at the transition region between the panel face and the panel skirt. This was done by decreasing (Run 62CH) or increasing (62DH) the Z-component of the Cartesian coordinates of all elements at the screen edge by 0.050 inches. The effects of these changes are shown in Fig. 21 and Table 5. The presence of a notch is seen to increase the stress to 1390 psi, while having additional glass at the transition region reduces the stress to 1266 psi. Calculations for the standard-design are also shown in Table 5.

In Table 5, it may be seen that the effect of having a decreased glass thickness at the screen edge increases the tensile stress by 86 psi. By comparison, increasing the thickness by 0.050 inches reduces the stress by only 38 psi. These results therefore emphasize the deleterious effects on the stress of having a notch in the region of the screen edge, compared to the smoother transition region of the standard panel design shown in Fig. 20.

3.5 Effect of a Reduced Funnel Thickness on Stress

A spun funnel is only about two thirds as thick as a pressed funnel. To determine the effect of a thinner funnel on the stress distribution, the previously-used pressed funnel model was reduced in thickness by $\frac{1}{3}$. The same standard panel was used as on the pressed funnel (Run 63C) described in the initial series of figures. The stress distribution for this bulb is shown in Fig. 22. Comparison with Fig. 7(b) shows that the stress at the screen edge is increased slightly to 1282 psi, compared to 1275 psi for the pressed funnel having the same panel. The stresses in the frit seal are increased to 910 psi, compared to 761 psi for the pressed funnel. The stresses in the thinner funnel are about 200 psi higher than in the pressed funnel.

The calculated stress distribution in the panel is compared with the

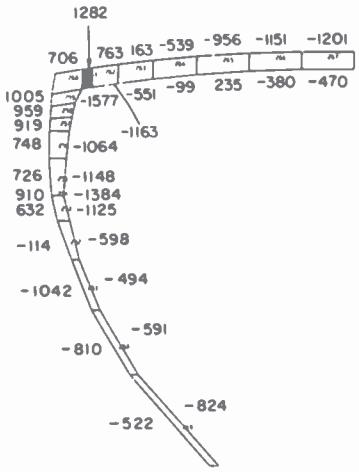

Fig. 22—Minor axis cross-section showing the stresses present in a standard panel on a thinner, spun-type funnel.

Table 6—Comparison of Calculated and Observed Principal Stresses in a Bulb having a thinner, spun-type funnel.

	Location on Panel	Calculated Stress 1 (psi)	Stress 2 (psi)	Distance (Inches)	Observed Stress 1 (psi)	Stress 2 (psi)	Distance (Inches)
1	Face Center (Vacuum Side)	−470	282	0	−478	319	0
2	Minor Axis	−380	301	2.3	−332	352	2.6
3	Major Axis	−378	279	2.3	−280	201	2.6
4	Major Axis	336	−15		388	89	6.8
5	Diagonal Axis	623	−272	6.4	687	−170	6.8
6	Major Axis	529	906	Screen Edge	638	912	Screen Edge
7	Major Axis	209	−1429	Inside Frit Seal	−59	−1212	Inside Seal Edge
8	Diagonal Axis	379	−103	Corner	408	−50	Corner
9	Minor Axis	1282	764	Screen Edge	1158	909	Screen Edge
10	Minor axis	−1384	−262	Inside Frit Seal	−1444	−26	Inside Seal Edge

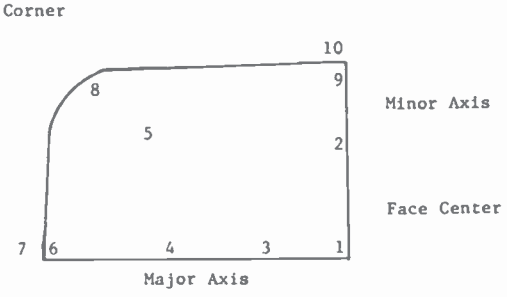

experimentally measured stress distribution in Table 6. In this Table, both principal stresses at each location have been included to indicate the degree of agreement. As can be seen, the values for the ANSYS calculated stresses and the strain-gage-measured stresses are in excellent agreement. This agreement further corroborates the accuracy and usefulness of the finite element method when a good model and a high order isoparametric element are used.

3.6 Effect of a Broad Seal Edge on Stress

In older-design funnels, the seal edge of the funnel was made deliberately wider than the panel seal edge to allow for manufacturing variability. In this way, the panel seal edge would always continuously contact the funnel seal edge even though the difference in interior dimensions may be 0.050 inches or more. The effect of one-sided seal-edge offset is considered in a later section.

The case of a wider-funnel seal edge was modeled by making the funnel 0.45 inches wide at the seal edge and tapering into the standard pressed-funnel model dimensions about 3 inches below the seal edge. The width of the panel seal edge is 0.35 inches. The frit seal material joined the panel and the funnel as shown in the inset to Fig. 23. Comparison of Fig. 23 with the standard bulb in Fig. 7(b) shows that the presence of the wider funnel seal edge does not appreciably alter the

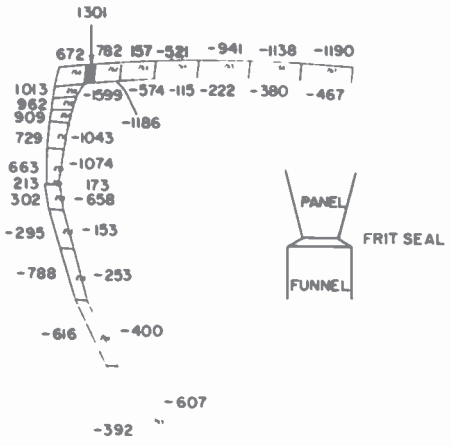

Fig. 23—Minor axis cross-section for a bulb having a 0.45 inch funnel and 0.35 inch panel seal edge. The centerface thickness is 0.500 inches. The inset shows the geometry of the seal edge.

stress distribution (by more than 25 psi) except in the region of the frit seal. The stresses are reduced in the frit seal and in the thickened region of the funnel presumably because of the larger cross-sectional area.

Thus, the principal advantage of the wider-funnel seal edge is the greater dimensional freedom it allows while assuring complete contact of the funnel and panel seal edges. In this way, manufacturability should be increased. Of course, the penalty is slightly increased weight of the funnel.

3.7 Effect of Offset Seal Edges on Stress

The effect of offsetting equally-wide (both are 0.35 inches) panel and funnel seal edges by 0.060 inches, is illustrated in Fig. 24. Here the stress in the frit seal increases to tensile values of 4216 psi for the funnel offset outward from the panel and to 3301 psi for the funnel offset inward from the panel edge. Needless to say, the magnitude is sufficiently high to be of concern. These high stresses could cause fracture of the weaker frit-seal material. Indeed, the frit seal has been observed to fail during the

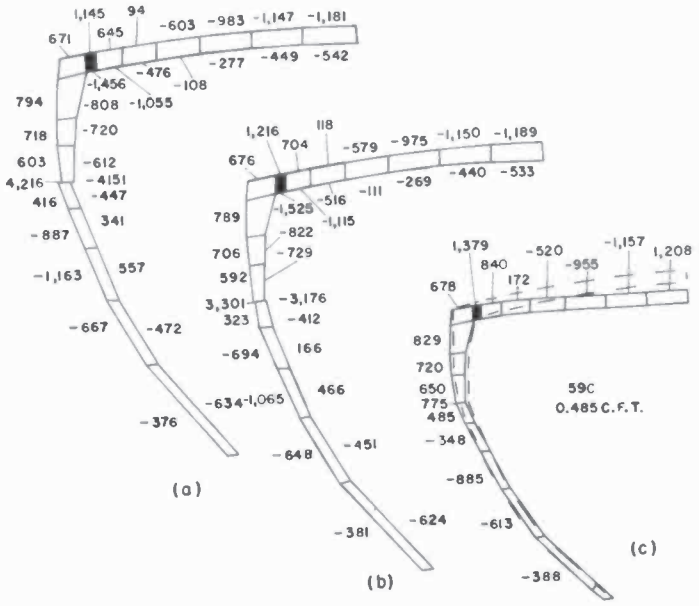

Fig. 24—Minor axis cross-sections of bulbs having a funnel that is displaced (a) outward or (b) inward by 0.060 inches relative to the panel. The standard bulb is shown in (c).

exhaust bake cycle (the bulb is first evacuated here) in some mismatched-seal-edge bulbs, confirming the high stresses calculated for the frit seal. Accordingly, it is of great importance that the seal edges be well matched to avoid failures during processing or at some later date.

As may be seen upon comparing the stress distributions for (a) and (b) in Fig. 24, the effect of a 0.060 inch inward or outward displacement of the funnel relative to the panel also changes the stresses at the screen edge. For comparison, a bulb having matched seal edges is shown in Fig. 24(c). Here the stress is 1379 psi at the screen edge and 775 psi at the frit seal. Thus, the outward displacement of the funnel reduces the screen-edge stress by 235 psi and the inward displacement reduces the stress by 160 psi. This reduction in stress comes about presumably because the funnel through the frit does not exert as great a downward and lateral restraint to the panel skirt as when the seal edges are matched. While the reduction in screen-edge stress is a desirable objective, achieving it by offsetting the seal edges is not an acceptable means, since the frit-seal stress is increased by a factor of 4 to 5 times compared to the matched case.

3.8 Effect of Tension Band Location on Stress

In one form of integral implosion protection, a steel tension band is placed around the skirt of the bulb after evacuation and final processing. Between this tension band and the glass is a steel rim band. During application of the tension band, it is pulled to about 1200 pounds force and then mechanically clamped together. The tension band is $\frac{5}{8}$ inches wide, 0.025 inches thick, made from high tensile strength steel, and is quite stiff. Accordingly, it does not apply a uniform force to the skirt periphery, but rather concentrates the inward-directed force at the corners. Therefore the action of the tension band was modeled by applying all of the force over three elements at the rounded portion of the panel corner. Axially, the location of the band can be adjusted from near the frit seal to near the viewing surface.

The effect of tension band placement on the calculated stress distribution is shown in Fig. 25. The inset on the right in the figure indicates the band position on the panel corner; near the face for band position between 3 and 2, and near the frit seal for band position between 2 and 1. The stresses for a band position near the face, Fig. 25(a) are generally lower than for a band positioned near the frit seal, Fig. 25(b). In particular, at the screen edge the stress is about 150 psi lower for the band placed near the face. This reduction in stress at the screen edge thereby provides an additional margin of safety against failure at the screen edge.

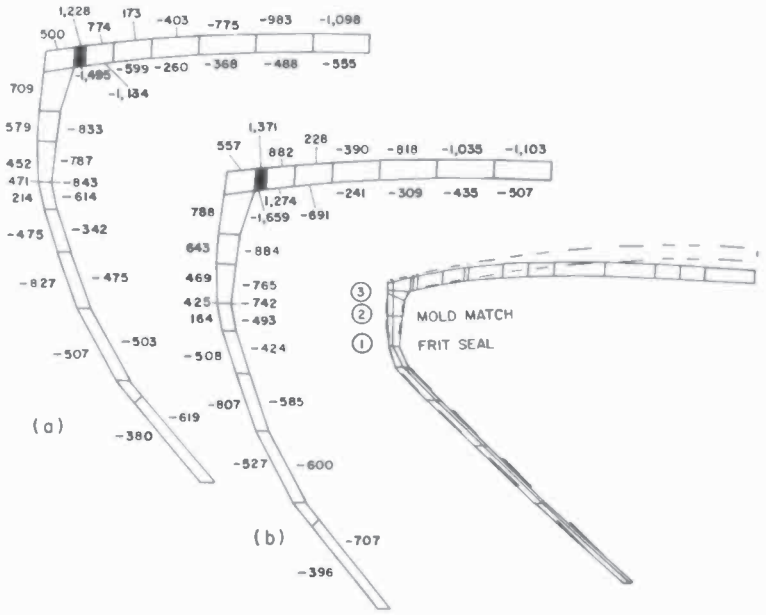

Fig. 25—Minor axis cross-sections of bulbs having (a) tension band between the face and the mold match, i.e., between 3 and 2 on the inset, and (b) tension band between the frit seal and the mold match, i.e., between 1 and 2 on the inset.

The stresses for a comparable unbanded tube were presented in Fig. 24(c). The screen-edge stress for the tube having the band near the frit seal is nearly identical to the unbanded tube. Accordingly, bands placed near the face appear to be preferable. Comparison with the unbanded tube also shows that banding reduces the stresses in the skirt, frit seal, and funnel by 200–300 psi, which is also desirable. But, stresses in the skirt and frit seal at the corner can be higher.

Finally, comparison of the displacement at the face center shows that the face moves inward about 0.002 inches less for the banded tube than for the unbanded one. This calculated difference agrees very well with values observed for actual tubes.[9]

3.9 Effect of Double Tension Bands on Stress

Another form of internal implosion protection utilizes two overlayed tension bands while omitting the rim band. In this version the bands are applied forward of the panel mold match near the viewing surface. Each band is tensioned to 1350 ± 150 pounds force. The cumulative effect of both bands is estimated to be 2250 pounds force (two times 1350 less

relaxation after the bands are clamped). Differences have been found between the implosion characteristics of bulbs having pressed versus the thinner spun funnels protected with double tension bands. In the Underwriters' Laboratory test, the thicker pressed funnel bulb has a satisfactory glass throw for a deliberately induced implosion, while the spun funnel bulb, as it presently is protected, does not meet the glass throw criteria. Accordingly, both a pressed and a spun-type funnel were modeled and compared to determine if the static stress distributions are different and whether this difference might explain the dynamic differences.

The static stress distributions calculated for the pressed and for the spun-type funnel are shown in Fig. 26 (A) and (B), respectively. These results may be compared with the nonbanded bulb in Fig. 7(c). Here we see that the stress at the screen edge is *reduced* by about 300 psi in both cases to about 960 psi. This effect is very beneficial in that by reducing the stress at the screen edge, it minimizes the deleterious effects of water-vapor-related stress corrosion on the safety of the tube.

The difference in the tensile stress distribution between the pressed and the spun funnels is about 30 psi on the face, a relatively small value,

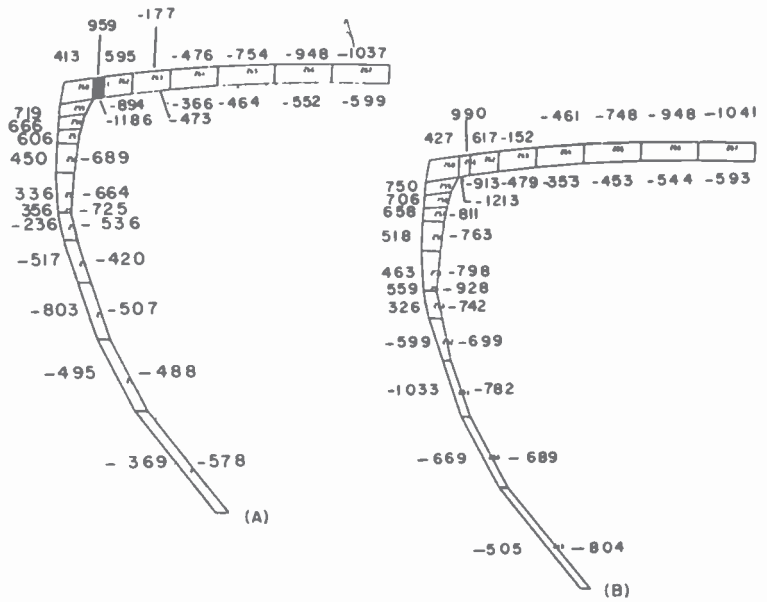

Fig. 26—Minor axis cross-sections for double tension bands on (A) pressed funnel and (B) spun, thinner funnel.

and about 200 psi in the frit seal region. In spite of the higher tensile stresses in the spun-type funnel, the frit seal, funnel, and skirt are not unduly stressed. Accordingly, since it appears that the static stress distribution is the same in both funnel types, differences noted in glass throw must be related to the dynamic behavior of the glass from the spun and pressed funnel bulbs.

3.10 Effect of Impact of the UL Missile on Stresses

In the Underwriters' test for glass throw upon implosion, a missile impacts the face of the screen with 15 foot-pounds of energy. To determine the effect of this impact on the stress distribution prior to rupture of the glass, the dynamic impact was approximated by a 7000 pound static force.[13] To determine the effect of impact on the glass itself, the bulb did not have an implosion protection band, as would ordinarily be present on a commercial tube.

The results of this calculation are shown in Fig. 27. Very high tensile stresses are shown to be present on the vacuum side of the tube near the point of impact (20,719 psi), along the atmospheric surface screen edge

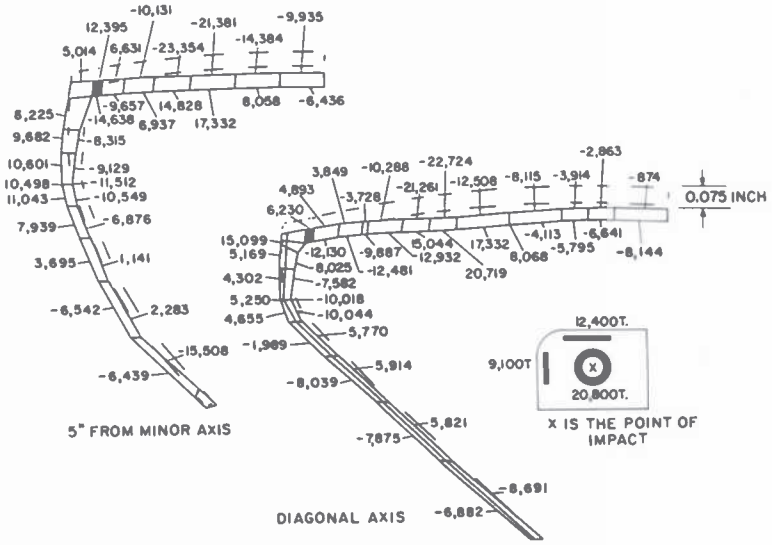

Fig. 27—Cross-sections through the minor axis 5 inches from face center (left) and through the diagonal axis (right) showing the stresses generated from a static force of 7,000 pounds. The inset shows the position of high tensile stresses on the tube face.

(up to 12,400 psi), and on the atmospheric surface of the skirt and frit seal region (up to 11,000 psi).* Thus, the calculation shows that several other high stress areas exist in addition to the point of impact. In turn, fracture during implosion testing is observed to occur at several locations, such as the screen edge, although the main fracture initially is the point of impact. At times, failure occurs in the funnel. The high tensile stresses generated by the impact cause a crack to be formed and this crack readily propagates in the tensile stress region. The atmospheric pressure opens up the crack, and complete failure then occurs.

The elastic deformation at the point of impact is about 0.075 inches as shown on the inset to Fig. 27. Simultaneously the frit-seal region moves outward 0.025 inches at the end of the minor axis and 0.015 inches at the end of the major axis. The deformation at the several locations is indicated by the difference between the original contour without atmospheric force or impact force, shown as a dotted line, and that for the deformed structure responding to the atmospheric and 7000-pound-impact force.

The exact correspondence of a 15 foot-pound impact and its static-force equivalent depends on a number of factors that are not unambiguous. Thus while one calculation gives 7000 pounds,[13] other calculations indicate that the force may be as high as 23,000 pounds.[14] In the latter case, the tensile stress around the point of impact would be very much higher than 20,000 psi and could be as high as 70,000 psi. It should be pointed out that the stresses indicated in Fig. 27 are *not* directly under the point of impact, but are the average value at a distance of about $\frac{3}{4}$ inch. Stresses at the point of impact would be much higher than the 20,000 or 70,000 psi discussed here. The present calculations are not intended to determine the highest stress at the point of impact, but rather to determine the location of high stress points all over the tube. To determine the value of the stress at the point of impact, a much smaller element size, perhaps as small as 0.050 inches on a side, should be used to resolve the stress in this high gradient region. Such a model has been used for the analysis of stresses in silicon wafers loaded with a point load at the center.[15]

A further refinement of the finite element calculation would be to determine the stress distribution when an implosion protection band is present. In this case, though, a simple approximation of the resultant force from the band acting on the diagonal axis corner could not be used, since the frit-seal region and skirt moves outward very significantly. Rather, a finite element model of the band, its position, and its applied

* Another calculation using stiff boundary conditions $UX = UY = UZ = 0$ to isolate the quarter symmetry section gives similarly high stresses at these locations.

load would have to be developed. The loaded tension band then would interact with the UL impact-simulating load on the face to restrict skirt and face movement. In this way the tensile stress region in the glass would be reduced, and glass fracture would not be be so catastrophic.

3.11 Effect of Thermal Gradients on the Stress Distribution

In the sections treated so far, the action of atmospheric pressure, band forces, and impact forces on tubes having various geometries has been examined. In this section we consider the effect of thermal gradients, such as might be developed during a high-temperature bake of the tube while it is being simultaneously evacuated. For these calculations, experimental values of the temperatures existing on the atmospheric and vacuum surfaces at about 50 locations[16] during the exhaust bake cycle were interpolated using a Lagrangian routine on a Hewlett-Packard 97 calculator for each of the 530 node points. The temperature at the center of the face was 350°C on the atmospheric side and about 312°C on the vacuum side. The gradient on both sides going towards the minor axis

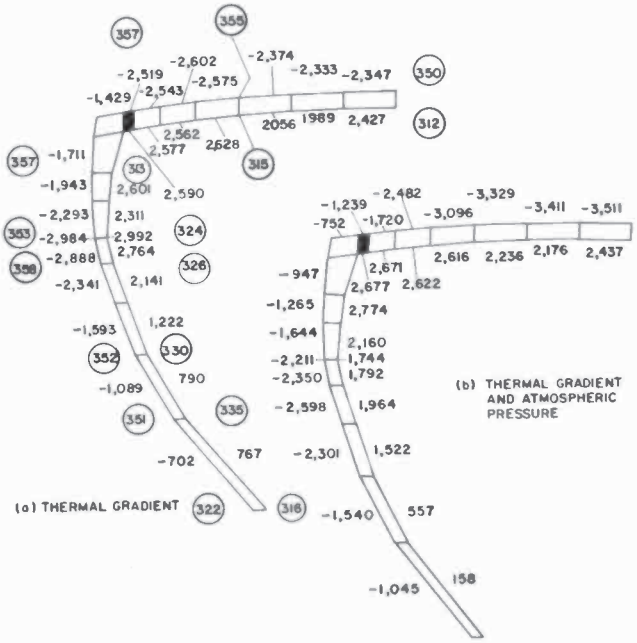

Fig. 28—Stresses induced (a) by thermal gradient and (b) by thermal gradient with atmospheric pressure. The thermocouple temperatures are circled. High tensile stresses exist along the inside surface of the tube for a higher outside than inside temperature distribution.

screen edge was about 7°C. The temperature differential between the inside and outside surfaces was about 44°C at the minor axis mold match, 30°C at the frit seal, and 6 to 20°C in the funnel.

The stress distributions resulting from the thermal gradient alone and in conjunction with the atmospheric pressure load are shown in Fig. 28. The temperature distribution as measured by thermocouples is shown by circled values. Here, a gradient of about 40°C exists between the outside and inside faces through the 0.485-inch-thick panel glass. Through the thinner sections of the funnel, the thermal gradient is much less. The tensile stresses on the vacuum side resulting from the thermal gradient are very high and range up to 2600 psi on the face and skirt and up to 2900 psi at the frit seal. The simultaneous application of atmospheric pressure reduces the tensile stresses in the frit seal by about 1200 psi (2922-1744 psi), which is good because the frit material can be weaker than the parent glass body.

In both (a) and (b) of Fig. 28, the entire outside surface including the screen edge is in compression. The outside surface is in compression principally because the outer surface is hotter and tries to expand. In so doing it puts the inside surface in tension. Fortunately, this high tensile stress is on the inside of the tube, removed from water vapor effects that can cause failure at lower stress levels by stress corrosion effects.

References

[1] R. W. Clough, "The Finite Element in Plane Stress Analysis," *Proc. 2nd A.S.C.E. Conf. on Electronic Computation*, Pittsburgh, Pa., Sept., 1960.

[2] O. C. Zienkiewicz, *The Finite Element Method*, 3rd ed., McGraw-Hill, London (1977) pp. 549–554.

[3] W. Visser, "A Finite Element Method for the Determination of Nonstationary Temperature Distribution and Thermal Deformations," *Proc. Conf. on Matrix Methods in Structural Mechanics*, Air Force Inst. Tech. Wright-Patterson A.F. Base, Ohio, 1965.

[4] J. O'Connor and J. Wang, "Finite element modeling of hydrodynamic circulation," in *Numerical Methods in Fluid Mechanics*, eds. C. Brebbia and J. O'Connor, Pentech Press (1974).

[5] R. H. Gallagher, *Finite Element Analysis Fundamentals*, Prentice-Hall, Englewood Cliffs, NJ (1975).

[6] E. L. Wilson, R. L. Taylor, W. P. Doherty, and J. Ghaboussi, *Numerical and Computer Methods in Structural Mechanics*, eds. S. J. Fenves, N. Perrone, A. Robinson and W. C. Schnobrich, Academic Press, N.Y. (1973) pp. 43–57.

[7] The ANSYS finite element software program used for the analysis of static, dynamic and thermal engineering problems was developed by John Swanson of Swanson Analysis Systems, Houston, Pa.

[8] J. H. R. M. Elst and D. K. Wielenga, "The Finite-Element Method and ASKA Program Applied in Stress Calculations for Television Picture Tubes," *Philips Tech. Rev.*, **37**, 56–71 (1977).

[9] G. Eiwen, private communication.

[10] As determined using an HP-97 calculator and program ME1-07A.

[11] R. J. Roark and W. C. Young, *Formulas for Stress and Strain*, 5th Ed., McGraw-Hill, N.Y. (1975), p. 386.

[12] Ibid, p. 392.

[13] S. T. Gulati, private communication.

[14] R. Shahbender, private communication.

[15] R. E. Enstrom and D. A. Doanne, "A Finite Element Solution for Stress and Deflection in a Centrally Loaded Silicon Wafer," to be published in the *Proceedings of the Symposium on Characterization Techniques for Semiconductor Materials and Science*, The Electrochemical Society, Princeton, N.J. (1978).

[16] J. Hale, private communication.